Physical Properties of γ Alumina Surface Hydroxyls Revisited through a Large Scale Periodic Quantum-Chemistry Approach

Anthony Dyan, Pierre Cenedese, and Pierre Dubot*

Laboratoire de Physico-chimie des Surfaces, Ecole Nationale Superieure de Chimie Paris, 11 rue Pierre et Marie Curie, 75231 Paris Cedex 05, France

Received: November 24, 2005; In Final Form: March 23, 2006

We have studied surface hydroxyls adsorbed onto (001), (011), and (111) γ alumina surfaces using a quantum-chemistry approach in order to compare with empirical models proposed in the literature. Local electronic structures and geometries in the low OH coverage limit have been evaluated for both ideal and relaxed surfaces with the help of a large scale periodic quantum-chemical code. Hydroxyl groups are adsorbed onto surfaces, and a study of their local electronic structure, vibrational frequencies, charges, and adsorption energies is performed and analyzed as a function of their adsorption site geometry. Our results show that, even on ideal (nonrelaxed) surfaces, OH local environments are more complicated than those stated by empirical models and strongly influence the hydroxyl stretching vibrational mode. Large scale simulation shows that disorder takes place even at 0 K, and the analysis of the vibrational frequencies leads to a revision of Knözinger's empirical model. Cationic vacancies in the first surface layers have also been taken into account; they have a significant influence on the surface atomic and electronic structures, modifying the physical properties of adsorbed OH entities. This work emphasizes the necessity to perform an electronic structure calculation to better understand adsorbed OH properties on γ alumina surfaces and reveals the difficulty to make a one-to-one correspondence between OH stretching frequencies and their other physical properties. Finally, we show that these results agree with some available experimental studies.

1. Introduction

Alumina is an important ceramic material for both applications and fundamental studies. It presents many phases among which α alumina and γ alumina are the most widely used. The α phase has been well characterized from crystallographic and electronic structure points of view both experimentally and theoretically; however, that is not the case for the γ one. Difficulties come from the unknown exact γ alumina spinel structure, as cationic vacancies must be introduced to recover stoichiometry. A controversial problem deals with the octahedral or tetrahedral nature of the vacancy sites and has been extensively discussed in the past decades. Both experimental[1,2] and theoretical (molecular dynamics[3−5] or density functional theory[6−8]) studies lead to opposite conclusions. The distribution of these defects, especially in the surface region, is crucial to understanding the surface restructuring and reactivity, and would justify a complete study in itself.

Characterization of the acidity−basicity of γ alumina surfaces and more precisely the surface site properties which govern the reactivity is a fundamental issue due to the wide application of γ alumina in catalysis. This has been mainly studied by infrared (IR) spectroscopy[9−12] in probe molecule adsorption experiments. Seven OH stretching bands have been observed in the spectral range above 3500 cm^{-1}. Since Peri's pioneering work,[13] empirical models proposed by Tsygnanenko and Filimonov,[10] Morterra et al.,[14] and Knözinger and Ratnasamy[9] aim to link each frequency with the local adsorption site geometry and coordination. These models are based on correlations between the "charges", the OH stretching frequencies, and the neighboring of both the OH groups and the cation involved in the adsorption. They conclude that the more the OH is coordinated, the lower the stretching frequency and the stronger the acidic behavior. Concerning the adsorption site geometry, this frequency lowering is also proposed when the cation coordination number decreases. These models use three low index ideal surfaces—(001), (011), and (111) (as obtained from cleavage of the bulk structure)—and lead to five hydroxyl stretching vibration bands, which is an interesting result compared to the model simplicity.

Later, Busca et al.[16] proposed another empirical model, which takes into account cationic vacancies onto the surface coupled with OH assignment for well-known and characterized compounds. This model modified in some way Knözinger's OH stretching frequency assignment. However, we should remark that this assignment based on a local adsorbing cation environment does not take into account the local chemistry (electronic structure) which is evidently not the same for different compounds with the same local structure. Moreover, let us mention that even if we trust this assignment based on a local adsorbing cation environment as proposed in most of the empirical models (bulk environment), none of them can a priori predict if any surface restructuring occurs.

Recently, Digne et al.[17,18] performed density functional theory (DFT) calculations on a different model of γ alumina structure with nonspinel site occupancy. In their study, the importance of morphology, temperature, and hydration of the surface is stressed. Their model leads to a novel assignment of the OH frequencies and suggests a significant revision of the Knözinger model. However, they do not use the same structure as the empirical model, and moreover, they do not consider the role of cationic vacancies in the surface layer. In addition, let us

* Corresponding author. E-mail: pierre-dubot@enscp.fr.

10.1021/jp056825i CCC: $33.50
Published on Web 05/03/2006

remark that none of the previously cited studies explain the singular reactivity of the OH site corresponding to the vibration at 3775 cm^{-1}, which is implied in acidic and basic adsorption processes.[15]

This work aims to study isolated adsorbed hydroxyl entities on low index γ-Al_2O_3 surfaces, to clarify the role of the real atomic structure (relaxation and cationic vacancies) and the electronic properties on their physical properties in relation to their catalytic activity, owing to the following constraints:

First, the calculations should apply to a thick 2D periodic slab, allowing a correct estimation of the semi-infinite medium electrostatic field on surface sites that can be monitored by checking that the Madelung potential in the heart of the slab matches its bulk value.

Second, the unit cell should be large enough so that the adsorbed OH low coverage limit is meaningful; in other worlds, the period should be large enough to avoid adsorbate−adsorbate interactions. Another advantage is it minimizes periodicity constraints in the surface plane so that short range surface ordering is not imposed.

Handling these constraints is not a simple task with ab initio methods such as QM, DFT, or high level post HF methods, while it remains tractable within the so-called semiempirical methods that merits and weaknesses are well established. Studies relative to molecular properties and reactivity have proved the good chemical accuracy of AM1 (and related theories) in a broad range of applications. To be convinced, a fair comparison, integrating several physical molecular observables, between common ab initio methods and AM1 can be done by consulting the remarkable NIST chemistry website. This paper is organized as follows. First, we check the ability of our large scale NDDO code handling unit cell of at least 500 (2 nm × 2 nm × 0.8 nm cell sizes) and up to 2000 atoms (4 nm × 4 nm × 0.8 nm cell sizes), to compute the bulk and surface alumina physical properties (electronic and atomic structures). Second, we study the Knözinger empirical model ideal surfaces and their adsorbed OH^- or H^+ entities for which we computed vibrational frequencies, charges, adsorption energies, O−H distances, and local density of states (LDOS). Finally, we release the constraints and optimize the atomic geometry in the three outermost surface planes to emphasize the effect of surface restructuring on the local properties for cationic ($Al^{\delta+}$, H^+) and anionic ($O^{\delta-}$, OH^-) surface sites.

2. Computational Method and Bulk Results

The calculations are based on our implementation of the semiempirical NDDO-AM1 method[19,20] with the molecular Fock equations carefully extended to 3D, 2D, and slab periodic systems in the direct space.[21] The Fock matrix is written by isolating the long range interactions and evaluating residual divergent terms through an Ewald summation.[22] To perform this summation, a small modification to the AM1 bielectronic integrals involving a monopole term have been made through averaging, making their asymptotic behavior independent of the atomic species. Periodic boundary conditions are applied by using the minimum convention image.[23] The self-consistent field problem is resolved using our original SQP algorithm[24] or our implementation of the trace resetting method.[25] Convergence criteria are met whenever the maximum commutator element absolute value is less than 10^{-5}, or a total energy variation fall below 10^{-8} hartree. Under these conditions, the charges are determined within an incertitude of $\pm 0.01e$. The geometry optimization is performed with a BFGS algorithm, and the equilibrium geometry is reached when the maximum gradient is less than 7×10^{-4} Hy/Å.

From a purely electronic description, AM1 is really well suited, giving a fairly accurate estimation of electronic structure (gap, vertical ionization energy, ...), which is ground information to deal with reactivity. Equilibrium geometries are quite satisfactorily predicted in regard to bond lengths and valence angles. The main drawback of this theory concerns the computation of the vibrational modes, which involve an empirical core−core repulsive energy, and it does not take into account anharmonicity. It is a common feature to characterize the relative merit of any method to predict vibrational properties through a scaling factor. It is very interesting to note that precomputed vibrational scaling factors over a large set of molecules gives a value of 0.954 for AM1, while, for comparison, we get 0.960 for B3LYP(6-31G*) and 0.967 in the case of B3LYP(6-311G**). Evidently, these are averaged values and a careful analysis on a specific molecule leads to a huge dispersion of some percent of ten. Similarly, in the following, we will use a constant biased scaling factor for the computed OH stretching frequency, corresponding to a shift of 240 cm^{-1}. It should be clear that our aim is to compute and compare OH stretching frequency shift for different local adsorption geometries, so this scaling factor is not crucial at all. To close this paragraph, we will mention that intrinsic difficulties arise when we deal with large systems independent of the level of the theory we use. In such systems, numerical instabilities prevent one from reaching fairly optimal geometries and even a fully converged density matrix, so the time-consuming analytical computation of the Hessian matrix is invariably inaccurate. The vibration frequencies that are proportional to the square root of the mass weighted Hessian eigenvalues are thus affected, so that numerical correction should be made.

The γ-Al_2O_3 surfaces are built from the $MgAl_2O_4$ spinel bulk structure. Magnesium atoms, located on the tetrahedral sites, are substituted by aluminum, and as mentioned before, cationic vacancies are generated in the cluster unit cell to restore the stoichiometry. In the following, the (O) and (T) configurations denote a crystal with only octahedral or tetrahedral cationic vacancies, respectively, while the (O,T) configuration corresponds to both vacancy types. In a first step, we have computed the energetically favored vacancy site occupation. We performed calculations on bulk γ alumina with a repeated 3D periodic 32-Al_2O_3 unit cell. The most stable configuration is obtained when all vacancies occupy octahedral sites (O) agreeing with DFT studies.[7] The energy difference between the (O) and (O,T) configurations is about 0.46 eV, whereas it is 1.84 eV between (T) and (O,T) (respectively 0.16 and 0.416 eV for DFT calculations). As we observed a weak energy difference between the (O) and (O,T) configurations, we have chosen to consider the (O,T) one in the following. Indeed, we believe that this difference is not significant if we consider the experimental conditions of γ alumina elaboration, as already mentioned in ref 7. We obtain a crystal structure with 68.2% of the cations in octahedral sites that is coherent with the experimental value ($70 \pm 2\%$) proposed by Lee et al.[26]

Crystal structural parameters of γ alumina were calculated, and we computed a unit cell volume which underestimates the experimental value by only 2%. We must emphasize here that we have used the AM1 parameters without performing any further optimization to reproduce observables with a better accuracy, stressing the good transferability of this NDDO approach.

The computed bulk electronic structure of γ alumina corresponds to an insulating oxide with a wide band gap of nearly 8.4 eV, whereas the experimental value is around 8.7 eV.[2]

Remember that DFT underestimates the band gap and gives results ranging between 4.8 and 5.1 eV[6] or in more recent work 3.9 eV.[27] In this work, energies will be referenced to the top of the upper valence band (UVB) corresponding to the highest occupied molecular orbital (HOMO) of the bulk electronic structure. The upper and lower valence band (LVB) widths are 11 and 9 eV, respectively, while experimental photoemission data estimate them to 10 and 6 eV.[2] In the UVB, three peaks appears at −2.2, −5.5, and −8.3 eV, while the experimental spectrum exhibits two main broad peaks at −3.2 and −5.5 eV. The UVB is well described, whereas the LVB is too broad and shifted toward lower energies. However, as we are mainly interested in surface chemical bonds, where frontier orbitals play a major role,[28] the LVB description is not so crucial and in any case will not influence the physics of our results.

Note that the main contribution to the UVB comes from oxygen 2p orbitals, while the LVB is dominated by their 2s orbitals. However, the contribution of the aluminum is not negligible in these valence bands, revealing both ionic and covalent bonding character rather than a purely ionic one. This result has been shown experimentally by Ealett et al.[2] through the Auger parameter measurement obtained from the Auger KLL oxygen lines, demonstrating local atomic charge variation for different alumina phases. This feature is displayed by the oxygen and aluminum computed local charges (−0.7*e* and +1.05*e*, respectively).

3. Surface Structure

The (001), (011), and (111) surfaces are the experimentally most stable faces,[29,30] and we will consider only these three low index surfaces. As in the empirical Knözinger model, we consider two terminations for each plane: (001) E,F; (011) C,D; and (111) A,B which are well described in refs 9 and 31.

In the first part of this work, we study OH properties on these ideal surfaces to compare our quantum approach with empirical model predictions and available DFT computations. For these surfaces, we locate the cationic vacancies on the opposite side of the ideal termination (model surfaces of type I). Then, in a second part, real surface studies are considered, where the vacancies are randomly distributed on both tetrahedral and octahedral sites on each plane of the cluster (model surfaces of type II). Of course, in this case, a geometry optimization is performed, leading to an atomic reorganization of the surface, as can be expected.[32,33]

4. Surface of Type I: Ideal Surfaces

4.1. Surface Electronic Properties. For each ideal surface, all possible adsorption site LDOS have been computed. We report in parts a and b of Figure 1 two cationic LDOS for an octahedral and a tetrahedral site, respectively, on the (001)E termination. The first has lost one neighbor out of six, while the second has lost two neighbors out of four.

For these two cationic sites, we note that the LVB is located at the same energy as that for the bulk electronic structure and extends from −30 to −21 eV. We also retrieve an UVB mainly centered at −5 eV. The LVB and UVB widths are smaller than the bulk ones owing to a lower coordination at the surface. The main difference between these two LDOS cationic sites appears in the upper part of the UVB at around 2.8 eV, which is important for the tetrahedral site and almost negligible for the octahedral one. This structure located at 2.8 eV falls in the bulk electronic band gap and mainly arises from hybridization of the 3s and 3p Al states with the 2s and 2p O states. An identical electronic surface state has also been observed (DFT) at the same energy by Ruberto et al. on κ alumina[34] and related to a dangling-bond character. The local electronic structure of this tetrahedral site shows a very small gap, while the octahedral one presents a reduced gap of nearly 3 eV.

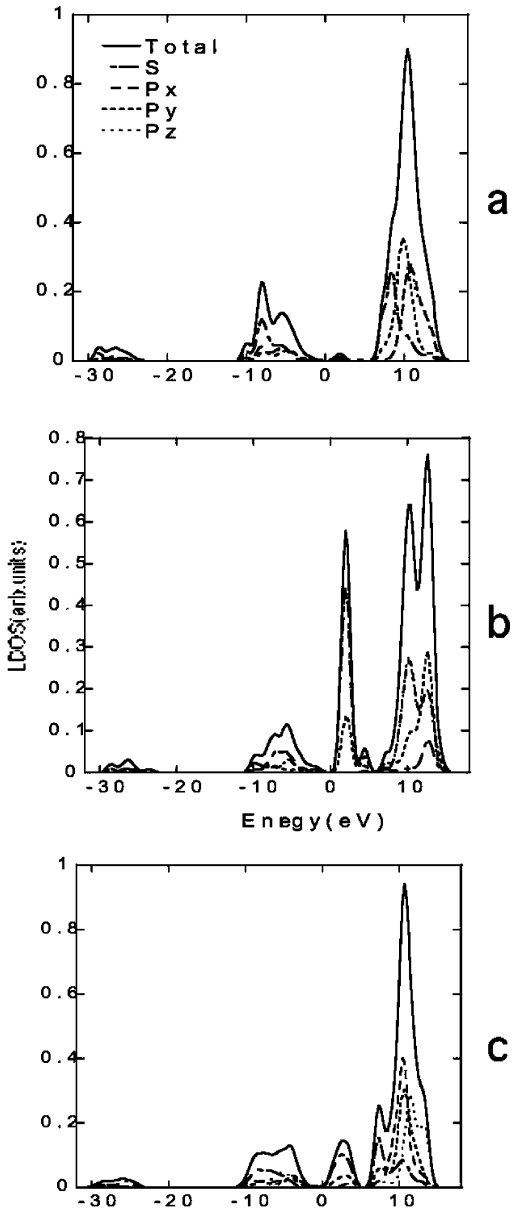

Figure 1. LDOS of a cationic octahedral (a) and tetrahedral (b) site of the (001)E surface. The LDOS for an octahedral site of the (011)C surface is also shown part c.

Consider now an octahedral site of the (011)C termination for which the LDOS is shown in Figure 1c. This octahedral site has lost two neighbors out of six, and once more, a small electronic surface state appears in the bulk band gap region.

For convenience, we do not present all of the computed LDOS, as they are very similar for other surfaces, and as a general rule, we find that the "weight" of the surface state is more important for higher unsaturated ions. This result indicates a first limitation of the empirical models, which do not take explicitly into account the tetrahedral or octahedral cationic site nearest neighbor number. As this local environment seems to strongly influence the LDOS, we can expect some effect on the adsorbed OH properties. Let us mention that the same trends as those for the cation LDOS are observed for anions.

4.2. OH^- or H^+ Entity Adsorption. For each of the six ideal planes, we considered all of the possible anionic and cationic

TABLE 1: OH Group Characteristics Associated with an Ideal Surface[a]

initial site	frequency (cm^{-1})	q_{OH}	d_{OH} (Å)	final site	charge	E_{ads,OH^-}	E_{ads,H^+}
$1t^2$ (122E)	3820	−0.304	0.95	$1t^1$	−0.25	6.7	7.4
$2o^5 1t^4$ (257E)	3531	−0.175	0.98	$1t^4 + 1o^4 +$ "$1t^4$" + "$1o^5$"	0.25	8.6	5.7
$1o^5$ (69E)	3786	−0.305	0.96	$1o^4$	−0.5	7.2	7.7
$1t^4$ (140F)	3800	−0.319	0.952	$1t^4 + 1H_O$	−0.25	2.6	9.3
$3o^5$ (284F)	3757	−0.351	0.953	$1o^4$	−0.5	6.7	11.1
$3o^5 1t^4$ (302F)	3439	−0.255	0.99	$2o^5 +$ "$1t^3$" + "$1t^4$" + $2H_O$	0	7.1	8.9
$1o^5$ (59F)	3789	−0.420	0.952	$1o^5$	−0.5	3.7	10.7
$2o^5 1t^4$ (194F)	3754	−0.292	0.956	$1t^3 +$ "$2o^5$"	−0.25	8.5	9.6
$1t^3$ (134C)	3657	−0.288	0.964	$1t^3 +$ "$1t^3$" + H_O	−0.25	7.5	7.7
$1t^3 2o^4$ (207C)	3732	−0.282	0.958	$1t^3 +$ "$2t^3$"	−0.25	8.4	6.6
$1o^4$ (88C)	3755	−0.275	0.957	$2o^4$	−0.5	8.2	8.5
$1t^4 1o^4$ (184D)	3673	−0.177	0.966	$1t^3 + 1o^3$	0.25	7.5	6.2
$1t^4 1o^4$ (263D)	3563	−0.200	0.978	$1t^3 + 1o^3 + H_O$	0.25	12.6	6.1
$1o^4$ (55D)	3778	−0.363	0.954	$1o^4$	−0.5	7.1	9.61
$3o^3 1t^4$ (211B)	3714	−0.269	0.981	$1t^4 +$ "$2o^4$" + 2"H_{Al}"	−0.25	9.31	6.6
$1o^3$ (23B)	3720	−0.228	0.958	$1o^3 +$ "$1o^3$"	−0.5	7.7	7.7
$1o^3$ (60B)	3721	−0.229	0.958	$1o^3 +$ "$1o^3$"	−0.5	7.3	8.0
$1o^3$ (90B)	3724	−0.237	0.957	$1o^3 +$ "$1o^3$"	−0.5	7.8	7.5
$1o^6$ (56A)	3671	−0.250	0.963	$2o^5$			
$1t^4$ (171A)	3603	−0.21	0.972	$2o^4 + H_O$	−0.25		

[a] Experimental OH stretching modes are observed in five spectral areas located at 3800, 3770, 3745, 3730, and 3700 cm^{-1}.

sites for H^+ and OH^- adsorption, respectively, leading to hydroxyl adsorbed entities. H^+ and OH^- adspecies were arbitrarily located at 0.3 nm above the adsorption site before beginning the geometry optimization. Then, we minimized the local geometry including moves of the nearest neighbors surrounding the adsorption site and performed a Hessian calculation to derive the vibrational frequencies.

Table 1 summarizes for each surface OH site considered in this work some of their main characteristics. The notation is the following: o^m and t^m symbolize OH entity connection to an octahedral or a tetrahedral site. The number before this letter gives the number of sites involved, whereas the exponent m indicates the number of nearest neighbor anions surrounding the cation. Finally, H_O symbolizes a hydrogen bond and the quotation marks symbolize a second neighbor interaction. For example, $2o^5 1t^4$ (site 257E in Table 1) accounts for a hydroxyl which is linked to two octahedral sites with five nearest oxygen neighbors and one tetrahedral site with four oxygen neighbors.

Let us carry out some remarks on the optimized geometries. The first concerns the OH entity orientation with respect to the surface. In contrast to the empirical model hypothesis, our calculation demonstrates that the OH axis is tilted from the normal. This leads to stronger chemical interactions with the surface, as hydrogen bonding can be effective. The second is the displacement of the OH entity from its ideal on-top location because the energy minimum can correspond to a bridged position. Note that the tilt of the adsorbed OH entity is not general and depends both on the surface orientation and on the adsorption site geometry. For example, considering the site number 257 of the (001)E surface, the adsorbed OH optimized position is with its molecular axis nearly perpendicular to the (001)E plane.

To outline the atomic displacements discussed above, we can see in Table 1 and in Figure 2 that the OH labeled 88 on the (011)C plane which was initially coordinated to only one octahedral site with four oxygen nearest neighbors is finally linked to two octahedral sites after geometry optimization.

In Figure 3, we have represented the vibrational frequencies versus the adsorbed OH equilibrium distance.

As proposed by the empirical models and observed in other electronic calculations,[17] the relationship between the OH distance and the vibrational frequencies is linear. Note here that when the OH entity is implicated in a hydrogen bond, the OH stretching frequency is lowered, as is well-known experimentally. The linear behavior shown in Figure 3 can be explained by considering the nonharmonic nature of the O−H bond. Nonharmonic contributions to the frequency are a function of d_{OH} and its powers. However, in the small range of d_{OH} values spanned in this study, we are only sensitive to the linear effect. Note that, in empirical models, the small O−H distances, that is, the high frequencies, are associated with a strong basic Bronsted character and a low OH adsorption energy. We will show later that even if we retrieve a linear correlation between O−H distance and OH stretching frequency, the link with OH adsorption energy is not clear.

We show in Figure 4 the linear decreasing behavior of the OH stretching frequency versus its average coordination. This behavior is in agreement with the fact that the lower the global OH charge, the higher the substrate−adsorbate charge transfer, with the latter being an increasing function of the nearest neighbor number.

We present in Figure 5 the OH stretching frequency versus the adsorption energy.

For Figure 5, no simple correlation can be drawn concerning the adsorption energy and the OH stretching. The difficulty to find a simple relationship between these two observables comes certainly from the adsorption energy definition, because it includes the surface nontrivial geometry optimization around the reactive site and very different local adsorption geometries. Indeed, the expression of the adsorption energy contains different contributions: electrostatic (Madelung), charge transfer, repulsion energy, and atomic reorganization. One can notice in Figure 5 that really different OH adsorption energies are associated with very similar OH stretching frequencies. These results agree with the experimental studies of Morterra[14,15] who pointed out that a straight correlation between OH reactivity and its vibrational frequency does not exist. This author discusses the difficulty to assign an acidic or a basic character for the hydroxyl vibrating at nearly 3775 cm^{-1} because it is implicated in surface reaction with both acidic and basic molecules, and it is not the highest nor the lowest frequency of the surface hydroxyls. The results we find here demonstrate that the assignment of the 3775 cm^{-1} stretching OH band to any acidic or basic surface reaction could correspond to different OH adsorbed species and not to a single entity with mixed acidic−basic properties.

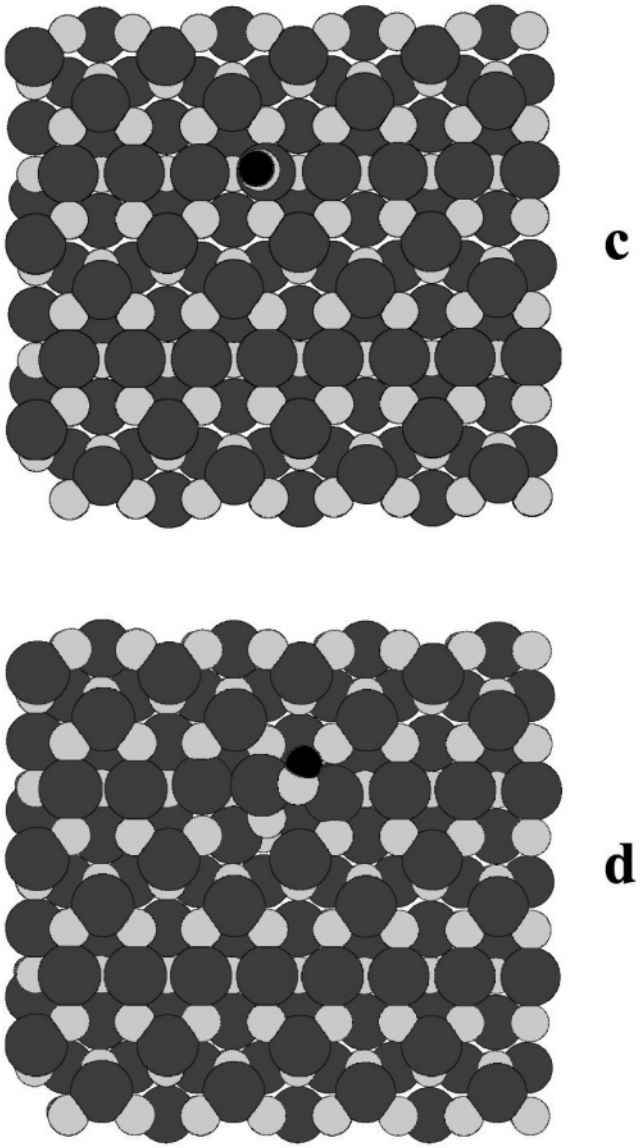

Figure 2. Top views for OH on the type I (011)C surface before (c) and after (d) geometry optimization. The large dark gray circles stand for aluminum, while the small light gray and small black circles stand for oxygen and hydrogen, respectively. Note in this figure the OH coordination change, which evolves from an on-top position to a bridged position during the geometry optimization.

Looking at Table 1, we can see that the lower the adsorbed OH charge, the higher its adsorption energy. We can also notice the F plane special behavior which presents the most basic OH sites. From our electronic structure calculation, we can explain the OH^- low adsorption energy on the F plane by its peculiar DOS energy position which is globally shifted by 4 eV with respect to the other surfaces. This shift increases the energy difference between ϵ_{LUMO}^{cation} and $\epsilon_{HOMO}^{OH^-}$ and by the way decreases the interaction energy. To outline this reasoning, a simple scheme can be used taking the first-order perturbation theory. Following Hoffman[28] and considering the chemical bond as conditioned by the frontier orbital characteristics, the strength of the interaction is given by

$$\Delta E = \frac{Z\beta^2}{|\epsilon_{HOMO} - \epsilon_{LUMO}|} \quad (1)$$

where Z is the coordination and β is the hopping integral. In our case, we consider the HOMO of the OH^- entity and the LUMO of the cationic site. Equation 1 shows that there is a competition between the number of neighbors and the HOMO−LUMO gap energy and that ΔE does not only imply the coordination number as proposed by the empirical models. Thus, the state appearing in the band gap region of the bulk structure, as well as UVB and lower conduction band (LCB) positions and related to cationic adsorption site geometry, has a significant influence on the OH entity properties, as demonstrated by the first part of this work.

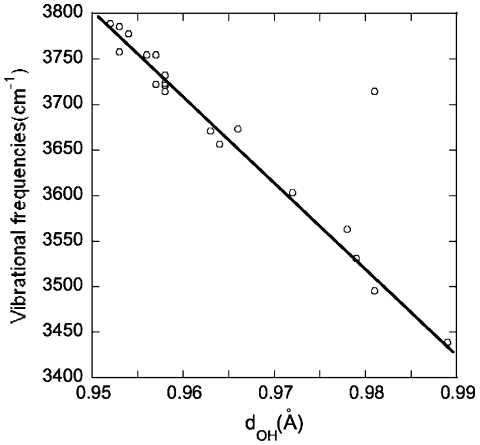

Figure 3. OH stretching frequency versus the OH bond length. This almost linear correlation, showing the well-known OH stretching frequency red shift with increasing interatomic distance, fully agrees with observed data and other computations.

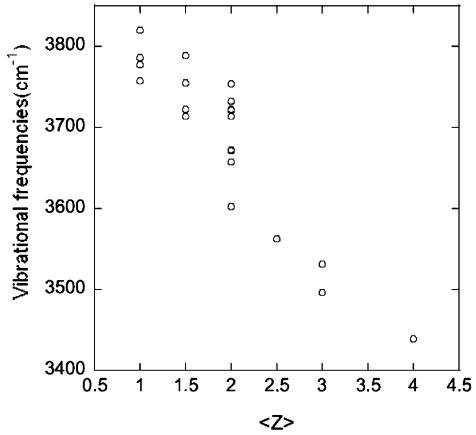

Figure 4. OH stretching frequency with respect to its average coordination showing that the higher the adsorbed OH coordination, the lower the stretching frequency.

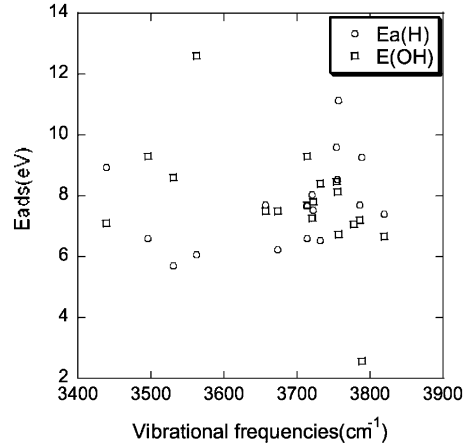

Figure 5. Hydroxyl adsorption energy versus its stretching frequency.

To summarize this discussion, we find that the higher frequencies correspond to OH^- adsorbed on surface cations, whereas the lower result from the adsorption of an H^+ entity adsorbed on surface anions in agreement with Noguera's work[35] for other oxides. Contrary to empirical model results, we observe that the vibrational frequency of an OH adsorbed on an octahedral site is lower than that for a tetrahedral one, confirming the recent Digne study.[17] Indeed, the empirical models link the OH frequency to the local adsorption site charge, which is determined by the electron delocalization between the neighbors. Thus, if the coordination number increases, the net charge on the OH is greater following the Pauling rules and the OH stretching frequency is higher. Our results show that this empirical reasoning does not hold and needs electronic structure calculations, with a characterization of the frontier orbitals implied in the adsorption process. As we also observe strong OH surface atomic displacements after local geometry optimization, assignment of OH stretching bands referred to a given compound structure (local environment) as is often done in empirical models could be even meaningless.

5. Surfaces of Type II: Fully Relaxed Surfaces

In the previous section, we observe a strong surface geometry disturbance in the vicinity of the adsorption site; thus, a complete study must take into account the whole surface restructuring in the initial state as well as that during the adsorption process. Moreover and as explained before, cationic vacancies must be introduced in the structure. They certainly play an important role in the surface optimized geometry and by the way onto the acid−basic properties of the surface. In this part of the work, cationic vacancies are randomly distributed on all of the cluster planes and only the atoms of the first three planes are allowed to move. Geometry optimization leads to strong surface reorganization with changes of local coordination for all six surfaces studied in this work. As a general rule for all faces, we observe surface disordering, as revealed by computing the partial radial distribution function which in our case has the shape of an amorphous system. Such a surface amorphization has been previously observed in molecular dynamics simulations[4,5] and also confirmed by the appearance of low coordinated cations found in experimental work.[1]

This disordering observed on both oxygen and aluminum rich terminated surfaces leads to local ionic charge dispersion and will be presented elsewhere.[36] As this paper is mainly focused on adsorbed OH properties, and in order to be concise, we only present here the surface structure and electronic property modifications for the (001)E plane, as similar behaviors are found on the other faces studied in this work.

Figure 6 summarizes the tendencies for the atomic structure geometry of the optimized cluster (001)E surface (cation rich surface plane). Ion valence electron number, coordinations, and altitude are displayed on the same graph. Altitudes are referenced to the nonoptimized surface plane position ($Z = 0$) and the initial altitude of the first three cluster atomic planes where the ions that are allowed to move are represented by horizontal lines. On this representation, we can see that ions are moved from their initial altitude positions by a relaxation phenomenon (displacement from the initial altitude materialized by horizontal lines). For cations belonging to the first and second surface planes, an important inward relaxation is observed (−0.04 and −0.02 nm, respectively), while, for the third plane, we have a small outward relaxation (less than +0.001 nm). In the case of anionic sites, we found an identical tendency for the outermost cluster plane, while two strong outward moves are observed

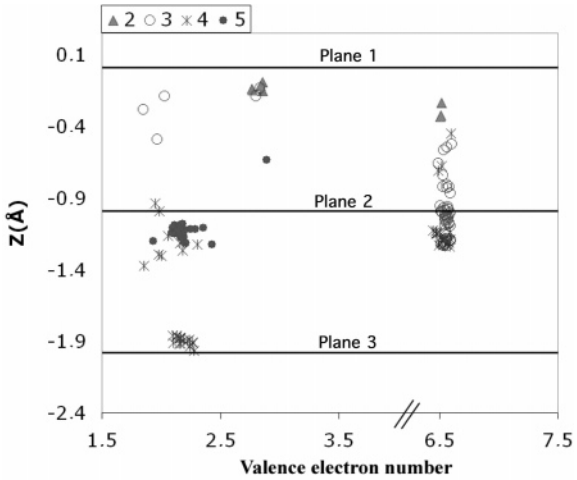

Figure 6. (001)E surface atomic structure after geometry optimization. The *x* coordinate corresponds to aluminum and oxygen valence electron number, while the *y* coordinate denotes ion altitude deviations from their location referenced to the initial surface first atomic plane. The symbols stand for the ion coordination, with dark triangles, circles, double crosses, and dark stars corresponding to two, three, four, and five coordinate species, respectively.

for the second and third cluster planes (+0.03 and +0.08 nm, respectively). We can also notice that altitude dispersion is more important for the planes closest to the surface in relation with surface disordering.

Concerning aluminum ion coordination, we found doubly coordinated (dark triangles) and triply coordinated (circles) ions in the ultimate surface layer, while in the ideal type I (001) surface only doubly and fifthly coordinated cations appear (see Figure 6). For oxygen, an average decrease of its coordination is also found, as we observe mainly doubly and triply coordinated ions in the topmost layer, while, on the ideal face, three and four coordinated species are present. These surface ion neighboring modifications are associated with ion charge variation, as could be expected. While the oxygen valence electron number stays around 6.6*e* (ion charge of −0.6*e*), this is not the case for aluminum ions. In fact, some of the surface cations located in the outermost surface plane show a strong increase of their valence electron number (nearly 2.80, while it is around 1.90 for a bulk species). This corresponds to a decrease of their local charge (+0.15*e* instead of +1.05*e*) and by the way diminishes the surface charge density for a cation rich surface plane.

5.1. Surface Electronic Properties. Full geometry optimization for the first three outermost planes of the cluster leads to a strong perturbation of the local ionic environment, as discussed in the previous section. As the local geometry changes between type I and type II surfaces, electronic properties and LDOS should be different.

In the case of the type II (001)E surface, we found that, for a tetrahedral surface cationic site far from a vacancy, the LDOS after relaxation is very similar to that of a type I surface (cations doubly coordinated appearing in Figure 6) and we found that the surface electronic state located in the bulk band gap remains present after geometry optimization. Main disparities are found when we consider the case of a site located near a vacancy for which the LDOS before and after geometry optimization are presented in Figure 7. Before geometry optimization, the LDOS presents an empty surface state located at 4 eV which is of course related to a cationic vacancy present in the site vicinity and is associated with a dangling-bond character. After geometry optimization, this state disappears, as can be seen, due to strong

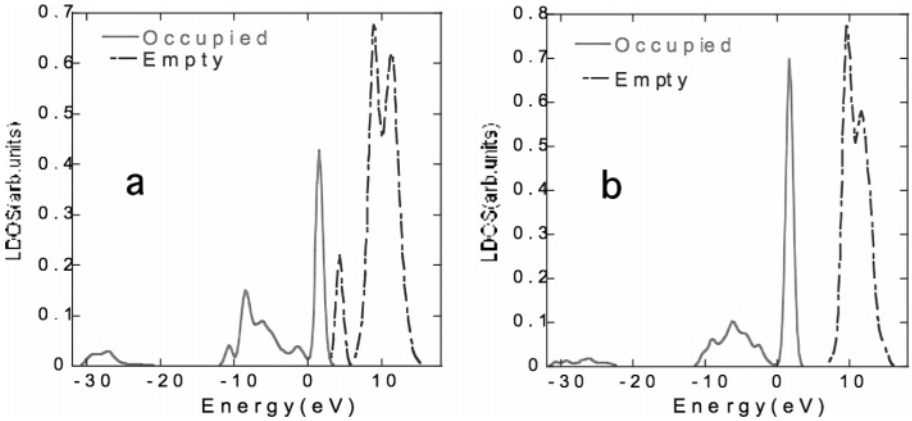

Figure 7. (a) LDOS of a cationic tetrahedral site of the (001)E surface near a vacancy before (a) and after (b) geometry optimization showing the effect of the adsorption site restructuring on the local surface state electronic structure.

TABLE 2: Calculated Physical Parameters for the Surface of Type II

face	frequency (cm^{-1})	q_{Al} or q_O	Z_{OH}	Z_{Al}	q_{OH}	E_{ads,OH^-}	E_{ads,H^+}	d_{OH} (Å)
124E	3816	+1.01	1	2	−0.28	7.8	8.9	0.953
116E	3783	+1.15	1	2	−0.28	9.7	7.9	0.958
60E	3772	+0.87	1	4	−0.30	9.0	6.8	0.960
126E	3749	+0.16	1	2	−0.25	8.7	7.3	0.957
121_dE	3724	+0.14	1	2	−0.23	8.1	9.0	0.958
50F	3766	+0.88	1	4	−0.33	10.6	4.5	0.957
53_dF	3740	+1.08	1	3	−0.27	10.5	6.4	0.960
326F	3678	−0.55	2	2	−0.33	8.8	7.8	0.967
142C	3795	+0.6	1	3	−0.28	8.3	8.4	0.952
108C	3784	+0.47	1	4	−0.32	8.3	7.7	0.955
154_dC	3761	+0.46	1	3	−0.28	8.8	8.3	0.957
101C	3735	+0.8	2	2	−0.24	9.1	6.2	0.960
74D	3749	+0.88	1	3	−0.31	11.3	5.5	0.957
53D	3730	+0.96	1	2	−0.30	11.2	5.3	0.959
439D	3612	−0.54	2	2	−0.13	8.7	7.7	0.968
44B	3817	+0.10	1	3	−0.25	8.5	9.4	0.956

atomic displacements near the cationic vacancy leading to coordination number homogenization smoothing bond deficiency for low coordinated surface ions. This surface reorganization is coupled with a surface charge density decrease, as mentioned previously, a well-known phenomena occurring on polar oxide surfaces.

As the LDOS seem to be modified by surface reorganization, and especially on sites located near vacancies, one can expect an effect on the adsorbed OH physical properties. Moreover, we showed in the previous section that the surface site's frontier orbitals are intimately implicated in the adsorbed hydroxyl characteristics, and as surface charge density modification shifts the electronic distribution (Hamiltonian diagonal term), we also expect OH adsorption energy modifications following eq 1.

5.2. OH^- or H^+ Entity Adsorption. OH^- or H^+ entities have been adsorbed on all of the surface sites following the same procedure as that for type I surfaces and after geometry optimization of clean surfaces. Contrary to type I surfaces, we cannot precisely characterize the local geometry of all sites mainly because the geometry optimization performed for each surface leads to disordering and only a statistic Al−O bond length distribution is meaningful. Thus, we analyze the different surface sites of each plane by considering their averaged coordination or local charge, as they could no longer be identified as purely octahedral or tetrahedral sites. For type II surfaces, the computed adsorbed hydroxyl observables are presented in Table 2. (No result is displayed for the A face due to the strong restructuring phenomenon observed on this highly polar surface that will be discussed elsewhere in a work focused on surface structure.[36])

One can observe in Table 2 that the OH stretching frequencies belong to the same spectral range, that the local charge distribution is nearly identical, and that the adsorption energies are of the same order. We can also notice both the homogenization of the interatomic distance and coordination of the OH group, with most of the adsorbed OH being connected to only one surface cationic site and being strongly tilted from the surface normal axis with an average angle of 65°. This is clearly different from type I surfaces where hydroxyls were connected to one, two, or three surface cationic sites, so let us now examine the main differences between hydroxyl distribution for type I and type II faces.

For the (001)E plane, we find high OH stretching frequencies in the range 3820−3750 cm^{-1} for an adsorption site far from a cationic vacancy, but we also find a lower frequency located at 3749 cm^{-1}. One can also notice that the low frequency located at 3531 cm^{-1} has disappeared. Considering the (001)F plane, we observe that the high frequency near 3800 cm^{-1} has been shifted to 3766 cm^{-1} and is still associated with an OH entity adsorbed onto a four coordinated cationic site. The lowest frequency which is close to 3439 cm^{-1} for the type I (001)F surface once more disappears, owing to surface restructuring.

On these two (001) surfaces, we have measured the effect of a vacancy in the vicinity of the adsorption site. A shift of nearly 26 cm^{-1} toward the lower frequency is found, as is observed for the site labeled 53 for the (001)F plane (site 50 when no defect is in the adsorbed OH vicinity). A molecular representation of an adsorbed OH on the site labeled 53 is shown in Figure 8, outlining the relaxed surface disordering. This frequency shift can be understood by considering the LDOS structure which presents a smaller gap when a vacancy is in the vicinity of the adsorption site. This leads to a smaller energy difference between the hydroxyl HOMO and the local cation LUMO, and by the way to a stronger hydroxyl−surface interaction, resulting in a smaller intramolecular bond in the adsorbed OH group. This frequency lowering due to surface vacancy is close to the one proposed by the Busca empirical model (lowering of 30 cm^{-1}). However, Busca's interpretation about the 3785 cm^{-1} frequency correlated with a vacancy nearby the adsorbed OH is not fully satisfying, as we obtain such a frequency for an OH adsorbed far from a cationic vacancy. Concerning the hydroxyl adsorption energies, we do not obtain the low values found for OH^- entities adsorbed onto the F plane type I surface, but we get the lowest H^+ adsorption energy (4.5 eV).

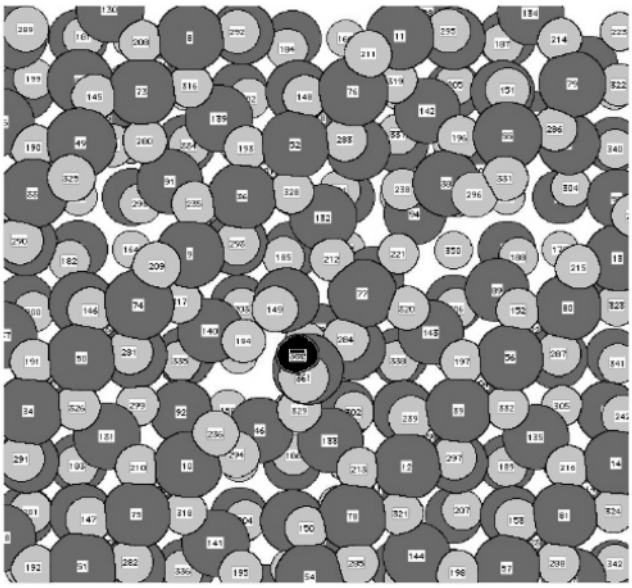

Figure 8. Molecular representation of the type II (001)F planes with an OH adsorbed onto the cationic site labeled 53. The large dark gray circles stand for aluminum, while the small light gray and small black circles stand for oxygen and hydrogen, respectively. Note the presence of nanopores and disorder compared with the ideal surface presented in Figure 2.

On the (011)C plane, two new frequencies are found (3784 and 3795 cm^{-1}) which are higher than those on the type I surface. For the(011)D plane, we do not find any OH frequency that matches those of the ideal surface. Let us remark that the OH adsorption energies on this plane remain the highest for OH^- and among the lowest for the H^+ (5.5 and 5.3 eV), over all of the cases studied in this work. Finally, we observe an OH stretching frequency homogenization for the (111)B plane and a strong increase of the 3720 cm^{-1} vibration mode to 3817 cm^{-1}, associated with the appearance of a weak cationic adsorption site charge (+0.1*e*).

Table 2 shows that the OH stretching frequency values are more dispersed on surfaces which are cation rich terminated (planes E and C) in correlation with a greater cationic site charge dispersion. One can also mention that it is for these terminations (E, C, and B) that we found the highest frequencies (>3780 cm^{-1}). We can also notice that the more coordinated the adsorbing cation, the lesser the OH stretching frequency dispersion (for a coordination of 2, frequencies are in the range 3730−3820 cm^{-1}, while, for a coordination of 4, it is in the range 3766−3784 cm^{-1}). This can be related to the fact that the lesser the cation coordination, the greater the disorder in the adsorbing site vicinity, and thus, the electron sharing between the cation and its neighbors is more dispersed.

To summarize the results presented in Table 2, our calculations clearly outline that the structural disorder observed on type II surfaces, and related to geometry optimization for clusters with cationic vacancies, strongly modifies the ν_{OH} distribution on the different surfaces. From these results, we can now search to see if correlations still exist between the computed hydroxyl observables, as has been done for type I surfaces.

As shown in Figure 9, we confirm the tendencies described in the case of the surface of type I concerning the relationship between the adsorbed OH stretching frequency and the OH distance, although as outlined before, atomic and electronic structures modifications lead to OH properties that are clearly different between type I and type II surfaces. This later remark is illustrated in Figure 10 where we can see that, for OH

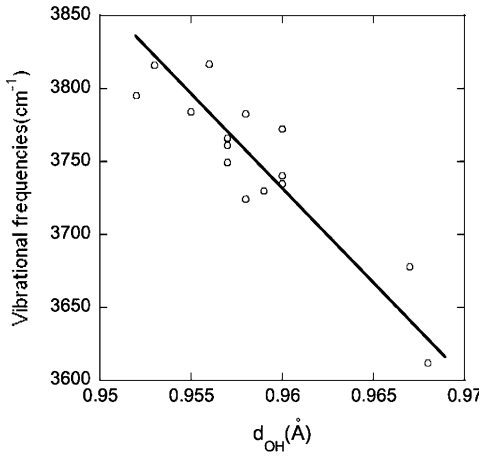

Figure 9. OH stretching frequency versus OH interatomic distance.

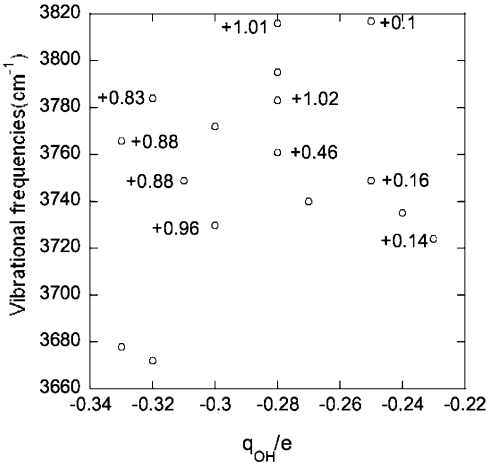

Figure 10. OH stretching frequency versus OH global charge. The cationic charge of the adsorption sites is shown near circles. This graph clearly outlines different adsorbed OH physical properties associated with the same OH stretching frequency.

adsorbed onto low coordinated cations (low ionic charge except for the 3780 cm^{-1} vibrational frequency), the global OH charge is lesser than that for those adsorbed on the high coordinated ones, while the OH frequency is identical. This confirms that on "real" surfaces, for a given adsorbed OH stretching frequency value, we may have different reactivities related to the adsorbed entity electron density.

Concerning the adsorption energies listed in Table 2, and plotted versus the OH stretching frequency in Figure 11, our calculation demonstrates that the highest values are for OH^- entities and the lowest are for the H^+. We emphasize that, in contrast to the case of type I surfaces, we observe a weak correlation, as in a rough approximation slopes are nearly constant, between the adsorption energies and the OH stretching frequencies.

Figure 11 shows that OH^- adsorption energy is a decreasing function of ν_{OH} while it is the contrary for proton adsorption. For surface hydroxyls characterized by a stretching frequency lower than 3780 cm^{-1}, we find that the H^+ adsorption energy is always lower than the OH^- one. We also notice that a greater adsorption energy dispersion is observed for low OH stretching frequencies.

Even if Figure 11 is cloudy, we may emphasize an interesting result. We see that the OH adsorption energy curve crosses the proton one near 3790 cm^{-1}, and is just below the highest value calculated in this work, so that this frequency can be associated

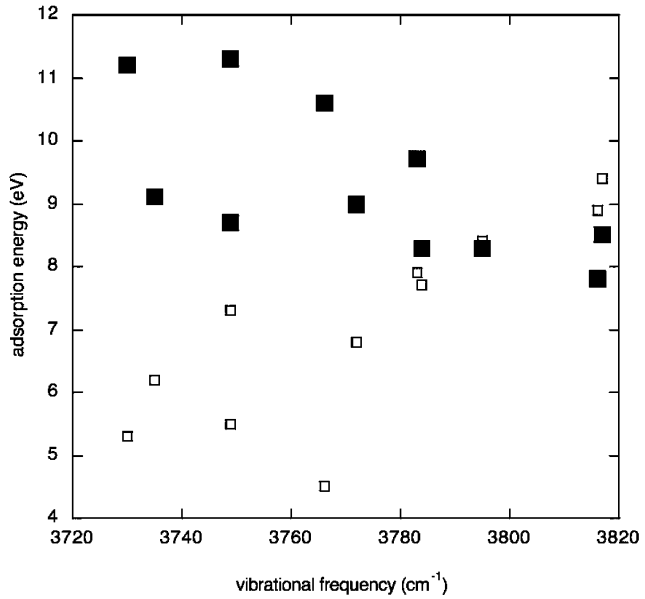

Figure 11. Adsorption energy for H^+ and OH^- entities versus the OH stretching frequency. The full black squares represent OH^-, and the small empty ones represent H^+. We clearly show in this figure the global trends of OH^- and H^+ adsorption energy which decreases with increasing ν_{OH} value for OH^-, while it is the opposite for H^+. Note the crossover around 3790 cm^{-1}.

with hydroxyls having both an acidic or a basic character. This result is to be brought closer to the particular reactivity of the hydroxyl(s) vibrating at 3775 cm^{-1} which is (are) implied in both acidic or basic surface reaction, as is found in probe molecule adsorption experiments.[9]

We must emphasize that it is difficult to associate a particular OH stretching frequency with a given surface orientation. Moreover, we remark that no strong correlations are found between OH vibration properties and its local coordination or the adsorbing cation local geometry (see Table 2), as the empirical models often suggests. This result could be a link to surface cation charge dispersion and to the lack of correlation between vibrational frequency and q_{OH}, as revealed in Figure 10, resulting from surface disorder which characterizes γ alumina surfaces.

We now compare our main results with available experimental ones. First of all, we can see that the adsorption energies of both H^+ and OH^- are of several electronvolts, revealing a weak Bronsted acidity and basicity for γ alumina. Concerning the low Bronsted basicity found in our work (high $E_{ads}^{H^+}$) for the most stable (011) faces, we can refer to the work of Morterra[38] concerning a pyridine adsorption experiment which showed that only coordinated pyridine is bound to the surface (no evidence of protonated species). By adsorbing the strongest bases such as NH_3, *N*-butylamine, or piperidine, Busca[39] confirms the low Bronsted acidity of γ alumina surfaces. Some other works showed that even if a complete proton transfer is not effective between the surface and the adsorbed pyridine molecule, hydrogen bonding can exist and the strength of this proton delocalization can be quantified by a red shift of the OH stretching frequency implied in such a bond. The work of Liu and Truist[40] shows that pyridine can be adsorbed on three different Lewis sites of the γ alumina surface, giving rise to hydrogen bonds with neighboring surface hydroxyls. Their results show that the most labile protons correspond to a surface OH vibrating near 3730 cm^{-1}, for which the red shift is around 360 cm^{-1}. This experimental result agrees with our calculation, as the more labile adsorbed protons for the most stable (011) surfaces are those labeled 74D and 53D in Table 2 for which we compute ν_{OH} values of 3749 and 3730 cm^{-1}, respectively. Note that, in a more recent study by Layman[41] using high resolution electron energy loss spectroscopy to probe γ alumina thin film reactivity, similar results were found. Those authors showed that the ν_{OH} close to 3711 cm^{-1} is shifted by H-bonding to lower frequencies. Note that two kinds of shifts exist, translating to two different surface hydroxyls vibrating at 3711 cm^{-1} with different proton labilities. Concerning the Bronsted basicity of γ alumina surfaces as outlined by Morterra,[38] CO_2 adsorption experiments reveal that the surface OH vibrating near 3775 cm^{-1} are the most reactive surface hydroxyls. Note that in Table 2 we observe the lowest $E_{ads}^{OH^-}$ for the most stable C and D planes mainly for hydroxyls characterized by ν_{OH} between 3761 and 3795 cm^{-1}. Another interesting work by Sahibed[44] confirms the spectral region of the most basic surface hydroxyls is near 3770 cm^{-1} by adsorbing CS_2 on γ alumina. To summarize, despite the fact that we use an NDDO approach, the physical results we get in this paper sound grounded, especially when we compare them to available experimental data.

6. Conclusion

We have investigated the vibrational and electronic properties of γ alumina surface hydroxyls in the framework of a homemade large scale NDDO periodic code with the aim to clarify the assignment of the ν_{OH} stretching frequency with local adsorption geometry and surface crystallographic orientation. To compare our results with empirical models often used to interpret experimental data, we have first probed different OH adsorption sites on ideal surfaces (no cationic vacancies, restriction of cluster surface atom displacements). Even in this ideal case (surface of type I), we found that the OH entity is not stable in the ideal position as arising from the bulk truncation, and total energy minimization often leads to a modification of the hydroxyl coordinance. From these previous results, we have in a second step computed the OH adsorbed geometry and electronic structure, leaving all of the cluster atoms of the first three surface planes free to move. Moreover, in this more realistic study (surface of type II), we distributed cationic vacancies needed to fit the γ alumina stoichiometry on all of the cluster planes. In this last case, strong local atomic position modifications are found and surfaces are disordered, leading to changes in the ν_{OH} stretching frequency distribution for all of the surfaces. Our study shows that the correlation between ν_{OH}, the local adsorption site geometry, and the adsorption energy of protons and hydroxyls is not so clear. Moreover, our results show that the assignment of OH stretching bands referred to a given compound structure or local environment of the adsorbed species, as is often done in empirical models, should be taken with care. We have compared the calculated ν_{OH} stretching frequency distribution and the associated adsorption energy for H^+ and OH^- with some experimental results in relation with the acidic−basic properties of γ alumina surfaces (probe molecule adsorption). We find that our results agree with experimental results: the most acidic surface hydroxyl groups vibrate near 3730 cm^{-1}, while the most basic ones are in the spectral range 3780 cm^{-1}. Nevertheless, we must be careful in the interpretation of the acidic−basic properties related to the OH entity adsorption energy as a dynamical study, taking into account the perturbation of the approaching reactant molecule on the surface properties, would be more meaningful.

In this work, we have focused our interest on the low coverage limit as it relates to a stronger catalytic activity. Now, it should

be interesting to study the effect of higher surface hydroxyl density on the surface structure and on the OH properties taking adsorbate−adsorbate interactions into account. Furthermore, these studies should be completed by introducing temperature effects that could affect the cation vacancy distribution in the surface region (short range order) and will be started soon.

References and Notes

(1) Zhou, R. S.; Snyder, R. L. *Acta Crystallogr., Sect. B* **1991**, *47* (*5*), 617.
(2) Ealet, B.; Elyakhlouffi, M. H.; Gillet, E.; Ricci, M. *Thin Solid Films* **1994**, *250*, 92.
(3) Gunji, I.; Teraishi, K.; Endou, A.; Miura, R.; Yin, X.; Yamauchi, R.; Kubo, M.; Chatterjee, A.; Miyamoto, A. *Appl. Surf. Sci.* **1998**, *130*−*132*, 549.
(4) Alvarez, L. J.; León, L. E.; Sanz, J. F.; Capitàn, M. J.; Odriozola, J. A. *Phys. Rev. B* **1994**, *50* (*4*), 2561.
(5) Blonski, S.; Garofalini, S. H. *Surf. Sci.* **1993**, *295*, 263.
(6) Mo, S.-D.; Xu, Y. N.; Ching, W. Y. *J. Am. Ceram. Soc.* **1997**, *80*, 1193.
(7) Guitiérrez, G. Taga, A.; Johansson, B. *Phys. Rev. B* **2001** *65* (*4*), 12101.
(8) Wolverton, C.; Hass, K. C. *Phys. Rev. B* **2000**, *653*, 24102.
(9) Knözinger, H.; Ratnasamy, P. *Catal. Rev. Sci. Eng.* **1978**, *17*, 31.
(10) Tsyganenko, A.; Filimonov, V. N. *J. Mol. Struct.* **1973**, *19*, 579.
(11) Morterra, C. *Proc. Sixth Int. Congr. Catal. (London)* **1976**, 194.
(12) Busca, G. *J. Catal.* **1991**, *131*, 167.
(13) Peri, J. B. *J. Phys. Chem.* **1965**, *69*, 220.
(14) Morterra, C.; Ghiotti, G.; Boccuzi, F.; Coluccia, S. *J. Catal.* **1978**, *51*, 299.
(15) Morterra, C.; Magnacca, G. *Catal. Today* **1996**, *27*, 497.
(16) Busca, G.; Lorenzelli, V.; Ramis, G.; Willey, R. *Langmuir* **1993**, *9*, 1492.
(17) Digne, M.; Sautet, P.; Raybaud, P.; Euzen, P.; Toulhoat, H. *J. Catal.* **2002**, *211*, 1.
(18) Digne, M.; Sautet, P.; Raybaud, P.; Euzen, P.; Toulhoat, H. *J. Catal.* **2004**, *226*, 54.
(19) Dewar, M. J. S.; Thiel, W. *Theor. Chim. Acta (Berlin)* **1977**, *46*, 89.
(20) Dewar, M. J. S.; Zoebisch, E. G.; Healy, E. F.; Stewart, J. J. P. *J. Am. Chem. Soc.* **1985**, *107*, 3902.
(21) Dyan, A.; Dubot, P.; Cenedese, P. Manuscript to be published.
(22) Ewald, P. P. *Ann. Phys.* **1921**, *64*, 253.
(23) Allen, M.; Tildesley, D. *Computer Simulation of Liquids*; Oxford University Press: New York, 1987.
(24) Dyan, A.; Dubot, P.; Cenedese, P. *Phys. Rev. B* **2005**, *72*, 125104.
(25) Niklasson, A. M. N.; Tymczak, C. J.; Challacombe, M. *J. Chem. Phys.* **2003**, *118* (19), 8611.
(26) Lee, M. H. *Chem. Phys. Lett.* **1997**, *265*, 673.
(27) Ahuja, R.; Osorio-Guillen, J. M.; Souza de Almeida, J.; Holm, B.; Ching, W. Y.; Johansson, B. *J. Phys.: Condens. Matter* **2004**, *16*, 2891.
(28) Hoffmann, R. *Solids and Surfaces: A chemist's View of Bonding in Extended Structures*; Wiley-VCH: New York, 1988.
(29) Beaufils, J. P.; Barbaux, Y. *J. Chim. Phys.* **1981**, *78*, 347.
(30) Nortier, P.; Fourre, P.; Saad, A. B. M.; Saur, O.; Lavalley, J. C. *Appl. Catal.* **1990**, *61*, 141.
(31) Tsyganenko, A.; Mardilovich, P. *J. Chem. Soc., Faraday Trans.* **1996**, *92*, 4843.
(32) Pinto, H. P.; Nieminen, R. M.; Elliott, S. D. *Phys. Rev. B* **2004**, *70* (12), 125402.
(33) Wallace, W. T.; Min, B. K.; Goodman, D. W. *J. Mol. Catal. A: Chem.* **2005**, *228*, 3.
(34) Ruberto, C.; Yourdshahyan, Y.; Lunddqvsit, B. I. *Phys. Rev. B* **2003**, *67*, 195412.
(35) Noguera, C. Physics and Chemistry of Oxide Surfaces. Cambridge University Press, 1996.
(36) Dyan, A.; Cenedese, P.; Dubot, P. Manuscript to be submitted for publication.
(37) Goniakowski, J.; Bouette-Russo, S.; Noguera, C. *Surf. Sci.* **1992**, *284*, 315.
(38) Moterra, C.; Magnacca, G.; deMaestri, P. P. *J. Catal.* **1995**, *152*, 384.
(39) Busca, G. *Phys. Chem. Chem. Phys.* **1999**, *1*, 723.
(40) Liu, X.; Truist, R. E. *J. Am. Chem. Soc.* **1997**, *119*, 9856.
(41) Layman, K. A.; Hemminger, J. C. *J. Catal.* **2004**, *222* (1), 207.
(42) Layman, K. A.; Ivey, M. M.; Hemminger, J. C. *J. Phys. Chem. B* **2003**, *107* (33), 8538.
(43) Zschack, P.; Cohen, J. B.; Chung, Y. W. *Surf. Sci.* **1992**, *262*, 395.
(44) Sahibed-Dine, A.; Aboulayt, A.; Bensitel, M.; Mohammed Saad, A. B.; Daturi, M.; Lavalley, J. C. *J. Mol. Catal. A: Chem.* **2000**, *162*, 125.